Undrained stability of a circular tunnel where the shear strength increases linearly with depth

Daniel W. Wilson, Andrew J. Abbo, Scott W. Sloan, and Andrei V. Lyamin

Abstract: This paper investigates the undrained stability of a plane strain circular tunnel in clay, where the shear strength profile is assumed to increase linearly with depth. Stability solutions for a variety of geometries and soil conditions are found using rigid-block upper bound methods as well as finite element limit analysis (which gives both upper and lower bounds). The latter procedures employ a discrete form of the bound theorems of classical plasticity, use a bespoke conic programming scheme to solve the resulting optimization problems, and bracket the true collapse load to within 5% for all the cases considered. Results from the study are summarized in the form of stability charts as well as an approximate closed-form expression that can be used by practising engineers.

Key words: tunnels, stability, limit analysis, finite element method.

Résumé : Cet article étudie la stabilité à l'état non drainé en déformation en plan d'un tunnel circulaire dans l'argile, dans lequel on considère que le profil de résistance au cisaillement augmente de façon linéaire avec la profondeur. Les solutions de stabilité pour une variété de géométries et de conditions de sol sont déterminées à l'aide de méthodes à frontière supérieure de blocs rigides, ainsi qu'avec les analyses par éléments finis (qui donne des frontières inférieures et supérieures). Ces dernières procédures impliquent une forme discrète des théorèmes des frontières de la plasticité classique, utilisent un code de programmation conique sur mesure afin de solutionner les problèmes d'optimisation, et donnent une valeur de la charge d'effondrement réelle à l'intérieur de 5% pour tous les cas considérés. Les résultats de l'étude sont résumés sous forme de tables de stabilité ainsi qu'en tant qu'expression fermée approximative qui peut être utilisée par les ingénieurs praticiens.

Mots-clés : tunnels, stabilité, analyse limite, méthode par éléments finis.

[Traduit par la Rédaction]

Introduction

This paper investigates the undrained stability of a circular tunnel in clay where the shear strength increases linearly with depth. The stability of the tunnel is found using numerical formulations of the limit analysis bound theorems as well as semianalytical rigid-block mechanisms. The problem considered, which assumes plane strain conditions, is shown in Fig. 1. The soil surrounding the tunnel is modelled as a heterogeneous Tresca material with a uniform unit weight (γ), a surface undrained strength (c_{u0}), and a fixed rate of strength increase (ρ) with depth (z). In most practical cases, the soil unit weight and the strength profile are known, and it is necessary to determine the values of the surface pressure and tunnel pressure that maintain stability. The undrained strength of the soil, c_u, at any given depth can be expressed as

$$[1] \qquad c_u(z) = c_{u0} + \rho z$$

where $\rho = 0$ corresponds to the homogeneous case with uniform strength. For undrained analysis, where deformation occurs at constant volume, it is convenient to describe the stability of a tunnel in terms of the dimensionless parameter $(\sigma_s - \sigma_t)/c_{u0}$, where σ_s is the surchage pressure applied to the ground surface and σ_t is the internal tunnel pressure (Sloan and Assadi 1992). This parameter is a function of the dimensionless variables H/D (where H is tunnel depth and D is the tunnel diameter), $\gamma D/c_{u0}$, and $\rho D/c_{u0}$ and be described by a function of the form

$$[2] \qquad N = \frac{\sigma_s - \sigma_t}{c_{u0}} = f\left(\frac{H}{D}, \frac{\gamma D}{c_{u0}}, \frac{\rho D}{c_{u0}}\right)$$

As the analytical solution for N is unknown, it is necessary to employ numerical methods to obtain approximate solutions that can be expressed conveniently in the form of dimensionless stability charts.

Upper and lower bounds on the stability parameter $(\sigma_s - \sigma_t)/c_{u0}$ of the tunnel shown in Fig. 1 are found by using finite element formulations of the limit theorems that are described in Lyamin and Sloan (2002*a*, 2002*b*) and Krabbenhoft et al. (2005, 2007). These techniques, which can model arbitrary geometries, layered deposits, and complex loading conditions, utilize linear finite elements to formulate an optimization problem that is solved using second-order conic programming. Safe estimates for the exact value of $(\sigma_s - \sigma_t)/c_{u0}$ are obtained using the lower bound theorem, which is based on the principle that any set of loads supported by a statically admissible stress field cannot exceed the true collapse load. Unconservative estimates of $(\sigma_s - \sigma_t)/c_{u0}$, on the

Received 2 September 2010. Accepted 8 April 2011. Published at www.nrcresearchpress.com/cgj on 31 August 2011.

D.W. Wilson, A.J. Abbo, S.W. Sloan, and A.V. Lyamin. Centre for Geotechnical and Materials Modelling, School of Engineering, University of Newcastle, Australia.

Corresponding author: Andrew J. Abbo (e-mail: Andrew.Abbo@newcastle.edu.au).

other hand, are found from the upper bound theorem, which states that the loads corresponding to the power dissipated by any kinematically admissible failure mechanism cannot be less than the true collapse load. Using both methods in tandem enables the true collapse load to be bracketed from above and below, with the true solution being known with more certainty as the accuracy of the bounds is increased. Upper bounds on $(\sigma_s - \sigma_t)/c_{u0}$ are also found using a semianalytical method, which optimizes the arrangement of a series of rigid blocks, separated by velocity discontinuities, to model the failure mechanism (see, for example, Chen 1975). These values, while useful in their own right, serve as a valuable check on the finite element limit analysis solutions.

Important analytical, numerical, and experimental investigations on the stability of circular tunnels in both purely cohesive and frictional soils include the work of Cairncross (1973), Atkinson and Cairncross (1973), Atkinson and Potts (1977), Mair (1979), Seneviratne (1979), and Davis et al. (1980). Following these studies, Muhlhaus (1985) derived an analytical lower bound solution for a plane strain circular tunnel and an unsupported tunnel heading in cohesive–frictional soil, while for the latter case, Leca and Dormieux (1990) derived both upper and lower bounds. Using finite element limit analysis, Sloan and Assadi (1992) published rigorous bounds for the case of a plane strain tunnel in a clay whose undrained shear strength increases linearly with depth, while Lyamin and Sloan (2000), using the same approach, derived bound solutions for the collapse of a plane strain circular tunnel in cohesive–frictional soil. There has been a limited amount of research into the stability of tunnel headings due to their complex geometry, which involves three-dimensional deformation. Treating the stability of a three-dimensional tunnel heading as a plane strain problem (in cross section) gives conservative solutions, and is therefore useful in practice. Chambon and Corté (1994) investigated the case of a three-dimensional tunnel heading in a cohesionless soil, while Augarde et al. (2003) investigated a plane strain heading problem in a purely cohesive soil, which is applicable to the stability of long rectangular galleries. The latter authors also discussed the validity of using a single number to describe tunnel stability.

The study undertaken in this paper is a major extension of the work originally published by Sloan and Assadi (1992). It covers a wider range of variables, develops an approximate equation for estimating the collapse pressure, and presents tighter bounds on the relevant stability parameter for all the cases considered. The significant increase in accuracy stems from the use of improved nonlinear optimization algorithms and the evolution of faster processors, with very large two-dimensional stability problems being solved in a matter of seconds.

Finite element limit analysis

The upper and lower bound theorems of plasticity are powerful tools for predicting the stability of geotechnical problems, but can be very cumbersome to apply in practice. Finite element formulations of these theorems, which have evolved markedly over the last two decades, provide a new and exciting means of applying them to complex engineering problems in a routine manner.

Formally, the lower bound theorem states that any stress field that satisfies equilibrium, the stress boundary conditions, and the yield criterion will support a load that does not exceed the true collapse load. Such a stress field is said to be *statically admissible* and is the quantity that must be found in a lower bound calculation. The upper bound theorem, in contrast, requires the determination of a *kinematically admissible* velocity field that satisfies the velocity boundary conditions and the plastic flow rule. For such a velocity field, an upper bound on the collapse load is found by equating the power expended by the external loads to the power dissipated internally by plastic deformation. Both limit theorems assume a perfectly plastic material with an associated flow rule, and ignore the effect of geometry changes.

Fig. 1. Plane strain circular tunnel in a heterogeneous Tresca material.

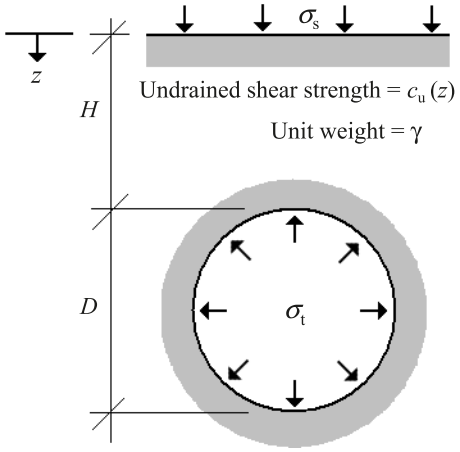

Finite element limit analysis is particularly powerful when upper and lower bound estimates are calculated in tandem, so that the true collapse load is bracketed from above and below. The difference between the two bounds then provides an exact measure of the discretization error in the solution, and can be used to refine the meshes until a suitably accurate estimate of the collapse load is found. The formulations used in this investigation stem from the methods originally developed by Sloan (1988, 1989), but have evolved significantly over the past two decades to incorporate the major improvements described in Lyamin and Sloan (2002*a*, 2002*b*) and Krabbenhoft et al. (2005, 2007). Key features of the methods include the use of linear finite elements to model the stress–velocity fields, and collapsed solid elements at all interelement boundaries to simulate stress–velocity discontinuities. The solutions from the lower bound formulation yield statically admissible stress fields, while those from the upper bound formulation furnish kinematically admissible velocity fields. This ensures that the solutions preserve the important bounding properties of the limit theorems.

For the tunnel shown in Fig. 1, the stability analysis proceeds by fixing values of H/D, $\gamma D/c_{u0}$, and $\rho D/c_{u0}$, with $D = c_{u0} = 1$ and $\sigma_s = 0$. This reduces the number of variables in the parametric study to the tunnel depth (H), the soil unit weight (γ), and the rate of strength increase with depth (ρ). An illustrative finite element mesh for the upper and lower bound analysis of a tunnel with $H/D = 1$ is shown in Fig. 2. Note that this mesh has been chosen for clarity only, and is much coarser than an actual mesh, which typically comprises

Fig. 2. Representative finite element mesh for $H/D = 1$ showing boundary conditions.

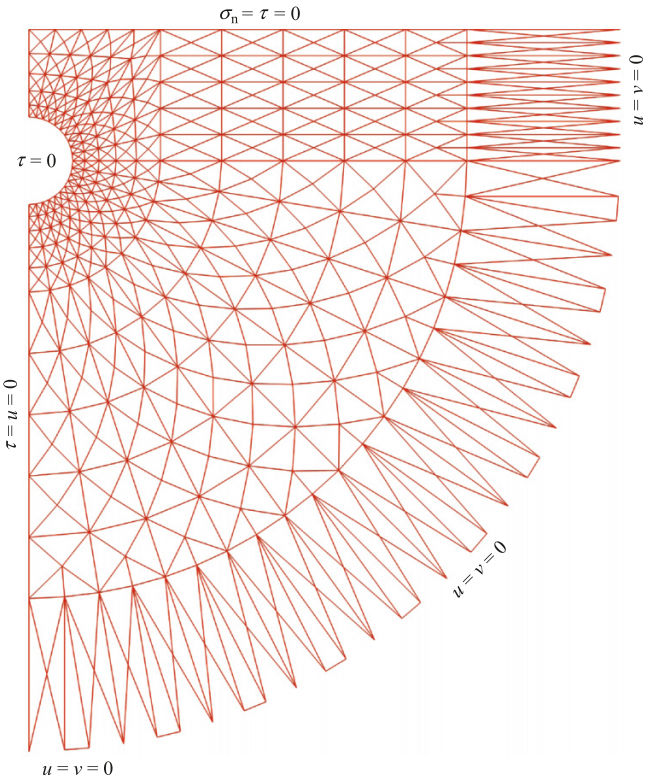

a minimum of 100 000 solid and discontiniuty elements. The grid is essentially the same for the upper and lower bound analyses, but the boundary conditions are set differently. To obtain the lower bounds, the normal and shear stresses (σ_n, τ) are prescribed as shown, while for the upper bound analyses, the appropriate kinematic restraints on the horizontal and vertical velocities (u, v) are set as indicated. In the lower bound analysis, the stresses are assumed to vary linearly over each triangle, and special extension elements are employed around the periphery of the mesh to extend the stress field throughout the soil layer. This latter feature is necessary to guarantee that the lower bounds are fully rigorous. In addition, statically admissible stress discontinuities are included at interelement boundaries, which means that several nodal points may share the same nodal coordinates but have different stresses. In the upper bound analysis, each triangle has a linearly varying velocity field and a constant stress field, with kinematically admissible velocity discontinuities at all interelement boundaries. For this case, several nodal points can again share the same nodal coordinates but have different velocities.

It is important to note that this paper investigates active collapse only, where failure is driven by the action of gravity and the surcharge pressure, with the resistance being provided by the internal tunnel pressure and the shear strength of the soil. The case of "blow-out", where failure is driven by the tunnel pressure and resisted by the action of the surcharge, gravity, and the shear strength, is not considered.

The lower bound analysis is performed by solving an optimization problem to find a statically admissible stress field that maximizes the quantity $(\sigma_s - \sigma_t)/c_{u0}$. Since σ_s is set to zero, this corresponds to finding the lowest tunnel pressure

Fig. 3. Rigid-block mechanisms used to find semianalytical upper bound solutions: (*a*) for shallow tunnels; (*b*) for deeper tunnels.

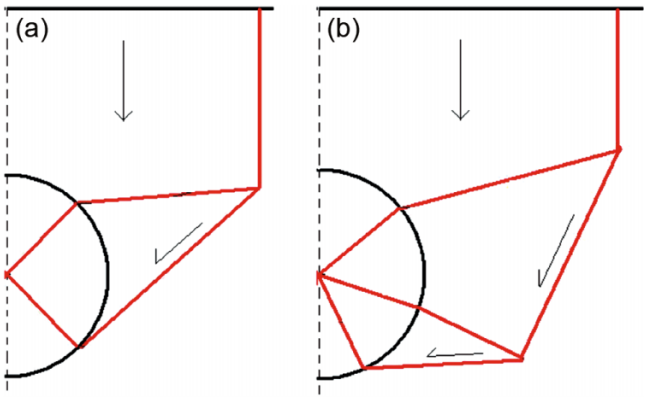

that just prevents collapse. In the upper bound analysis, the work expended by the uniform external tractions and unit weight is given by

$$[3] \qquad -\int_{A_t} \sigma_t v_n \, dA + \int_V \gamma v \, dV = -\sigma_t \int_{A_t} v_n \, dA + \gamma \int_V v \, dV$$

where A_t is the area of the inside of the tunnel subject to σ_t, v_n is the normal velocity acting over the inside of the tunnel, V is the volume of the soil mass, and v is the vertical velocity (positive downwards). Equating this to the internal power dissipation, P_{int}, and rearranging gives

$$[4] \qquad -\sigma_t = P_{int} - \gamma \int_V v \, dV$$

where the boundary condition $\int_{A_t} v_n \, dA = 1$ is imposed to initiate collapse. By minimizing the terms on the right-hand side of the above equation an upper bound on $(\sigma_s - \sigma_t)/c_{u0}$ is obtained.

Rigid-block analysis

Semianalytical rigid-block analyses were also used to determine upper bound estimates for the collapse load of the circular tunnels. As expected, these estimates were slightly above those from finite element limit analysis, as the latter permit plastic deformation throughout the soil mass and not just in velocity discontinuities. The two mechanisms considered in the rigid-block analyses are shown in Fig. 3. Upper bounds on $(\sigma_s - \sigma_t)/c_{u0}$ for these cases were obtained by imposing a unit downwards velocity on the upper block and then using the associated hodograph, coupled with the Hooke–Jeeves optimization algorithm (Hooke and Jeeves 1961), to minimize the dissipated power. At all times in the optimization process, a simple penalty function approach was used to ensure that the discontinuity lengths and block volumes were nonnegative.

These analyses are extremely quick and, for some tunnel geometries, provide a reasonably accurate upper bound on the true collapse load.

Results and discussion

The stability of a single circular tunnel, for dimensionless tunnel depths ranging from $H/D = 1$ to $H/D = 10$, are sum-

marized in Figs. 4–8 and Tables A1 and A2 in Appendix A. These charts plot the stability parameter $(\sigma_s - \sigma_t)/c_{u0}$ versus the dimensionless unit weight $\gamma D/c_{u0}$ for various values of the soil strength factor ($\rho D/c_{u0}$). Note that, due to its definition, a negative value of $(\sigma_s - \sigma_t)/c_u$ implies that a compressive normal stress must be applied to the wall of the tunnel to support a surcharge pressure, while a positive value of $(\sigma_s - \sigma_t)/c_u$ means that in some cases no tunnel support is required (in fact the tunnel may even support a negative pressure and still not collapse). The points at which the charts cross the horizontal axis define the configurations for which the tunnel pressure must match the surcharge to prevent collapse. For these special cases, if σ_s is zero, no tunnel pressure is needed to maintain stability.

The finite element upper and lower bounds lie, for the most part, within a few percent of each other for the full range of cases considered. The upper bounds from the rigid-block mechanisms give good estimates of $(\sigma_s - \sigma_t)/c_{u0}$ for shallow tunnels, where the rate of strength increase is small, but become increasingly inaccurate as this quantity increases for deeper tunnels. For shallow tunnels where $H/D \leq 2$, the optimal rigid-block mechanism is that shown in Fig. 3*a*, which involves failure through the roof and sides of the tunnel. With deeper tunnels, the failure zone extends through the base of the tunnel and reflects the mechanism for deeper tunnels as shown in Fig. 3*b*.

For shallow tunnels in a homogeneous soil with a small unit weight, the failure mode is typically confined to the upper half of the tunnel. This can be seen in Fig. 9, which shows the power dissipation intensity and the velocity field at collapse for a case with $H/D = 1$, $\gamma D/c_{u0} = 0$, and $\rho D/c_{u0} = 0$.

As expected, when the shear strength increases linearly with depth, failure occurs in the weakest material and is much more localized. In general, this leads to shallow and narrow failure mechanisms, as shown in Fig. 10 for the case where $H/D = 1$, $\gamma D/c_{u0} = 0$, and $\rho D/c_{u0} = 1$. Due to the fact that $(\sigma_s - \sigma_t) > 0$ for all cases where $\gamma = 0$ in Figs. 4–8, collapse can only occur with a weightless soil and no surcharge loading when a tensile pressure is applied to the tunnel wall.

Unsurprisingly, for moderately deep tunnels in a homogeneous soil with a high unit weight, the collapse mechanism is more extensive and often results in floor heave. This is illustrated in Fig. 11 for the case where $H/D = 4$, $\gamma D/c_{u0} = 3$, and $\rho D/c_{u0} = 0$. These deeper collapse mechanisms are more complex than their shallower counterparts, which explains why the rigid-block upper bounds are generally more accurate for shallow tunnels.

Once the strength of the soil increases with depth, the collapse mechanism for moderately deep tunnels again becomes more localized and does not cause floor heave. This behaviour can be seen in Fig. 12, which shows the failure mode for a case with $H/D = 4$, $\gamma D/c_{u0} = 3$, and $\rho D/c_{u0} = 1$. Compared to the homogeneous-strength example shown in Fig. 11, the lateral extent of the collapse zone is much reduced, and there is no plastic deformation below the floor of the tunnel.

The behaviour for deep tunnels is similar to that of their shallow counterparts, and is shown in Figs. 13–16 for cases with $H/D = 7$ and $H/D = 10$.

Bound solutions for a plane strain circular tunnel in undrained clay with a uniform shear strength have been given by Mair (1979) and Davis et al. (1980). Using an early variant of finite element limit analysis based on linear programming, Sloan and Assadi (1992) improved the accuracy of these bounds and also considered the important case where the strength increases linearly with depth. Figure 17 shows a comparison between the new results, the experimental centrifuge results of Mair (1979), and the predictions obtained by Sloan and Assadi (1992) for a homogeneous case. For this example, the $\gamma D/c_{u0}$ parameter is equal to 2.6, and the values for Sloan and Assadi (1992) were found by interpolation between $\gamma D/c_{u0} = 2$ and 3. The centrifuge data of Mair (1979) are still one of the most comprehensive sets of experimental results available, and were performed in a soil with a relatively uniform strength profile.

Figure 17 shows that the new predictions are in close agreement with Mair's centrifuge measurements, as well as being a significant improvement on the results of Sloan and Assadi (1992). A further comparison of the new results with those of Sloan and Assadi (1992) is given in Fig. 18 for a tunnel in heterogeneous soil with $H/D = 4$. This figure indicates that the new bounds give the greatest improvement over the old bounds for cases where the strength increases rapidly with depth.

Design formula

A parametric equation can be developed to describe the undrained stability of a circular tunnel in terms of the three dimensionless variables $\gamma D/c_{u0}$, H/D, and $\rho D/c_{u0}$. From Figs. 4 to 8 we see that the stability can be considered as linearly proportional to $\gamma D/c_{u.}$ Adopting this assumption, the stability parameter can be expressed in the form

$$[5] \qquad N = N_0 + \left(\frac{\gamma D}{c_{u0}}\right) N_\gamma$$

where N_0 is the stability number for the weightless case (i.e., $\gamma D/c_{u0} = 0$), N_γ is a factor accounting for the weight of the soil, and both these factors are nonlinear functions of the parameters H/D and $\rho D/c_{u0}$. Fitting a curve to the all finite element results for the weightless cases gives

$$[6] \qquad N_0 = 2\left(\frac{\rho D}{c_{u0}}\right)\left(\frac{H}{D}\right)^{\sqrt{2}} + 1.5\ln\left(\frac{H}{D}\right) + 2.4$$

A graphical representation of this equation, which is a more convenient form for use in design, is presented in Fig. 19. Numerical values for N_0 can be found in Table A3 of Appendix A.

Using parametric curve-fitting techniques to fit eqs. [5] and [6] to the lower bounds from the finite element limit analysis, an expression for the factor N_γ is obtained as

$$[7] \qquad N_\gamma = \begin{cases} N_\gamma = -1.05\left(\dfrac{H}{D}\right) - 0.3 & \left(\dfrac{\rho D}{c_{u0}}\right) < 0.15 \\ -1.01\left(\dfrac{H}{D}\right) - 0.24 & \left(\dfrac{\rho D}{c_{u0}}\right) \geq 0.15 \end{cases}$$

For the case of $\gamma D/c_{u0} = 2$, Fig. 20 shows that the stability parameters predicted from the approximate eqs. [5]–[7]

Fig. 4. Results for (*a*) $H/D = 1$; (*b*) $H/D = 2$. FEM, finite element method; RB, rigid block.

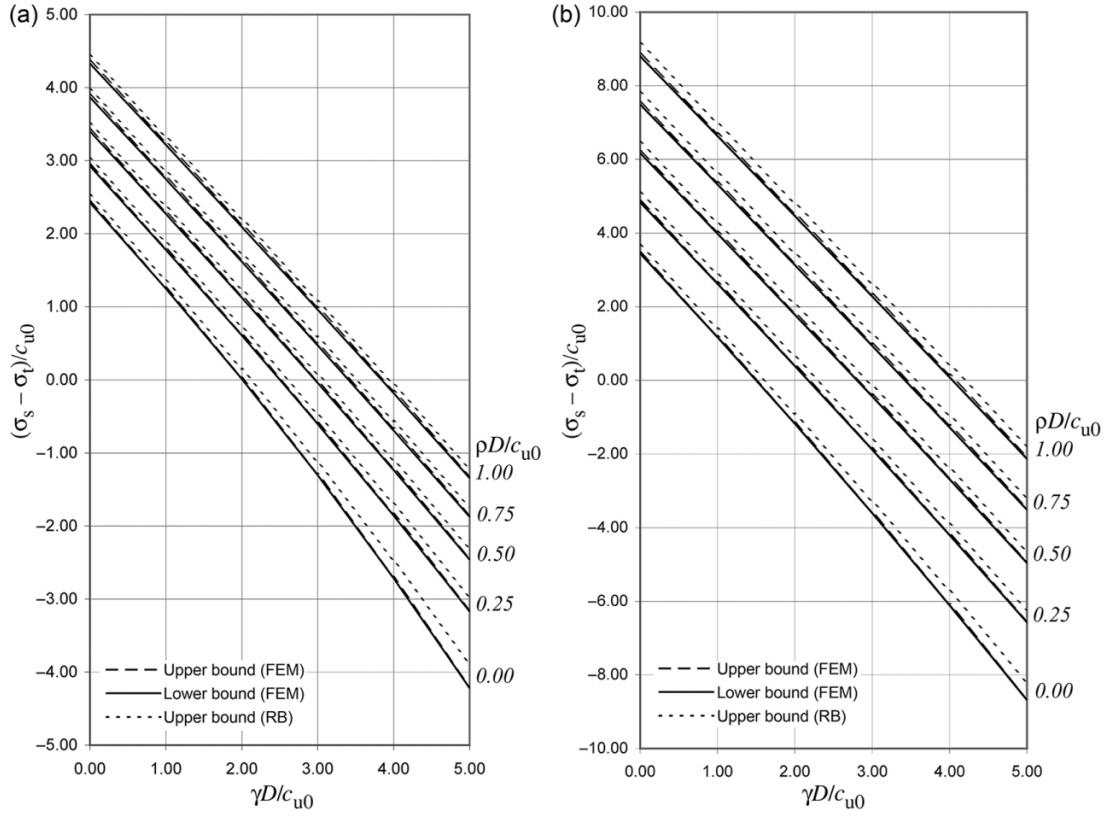

Fig. 5. Results for (*a*) $H/D = 3$; (*b*) $H/D = 4$.

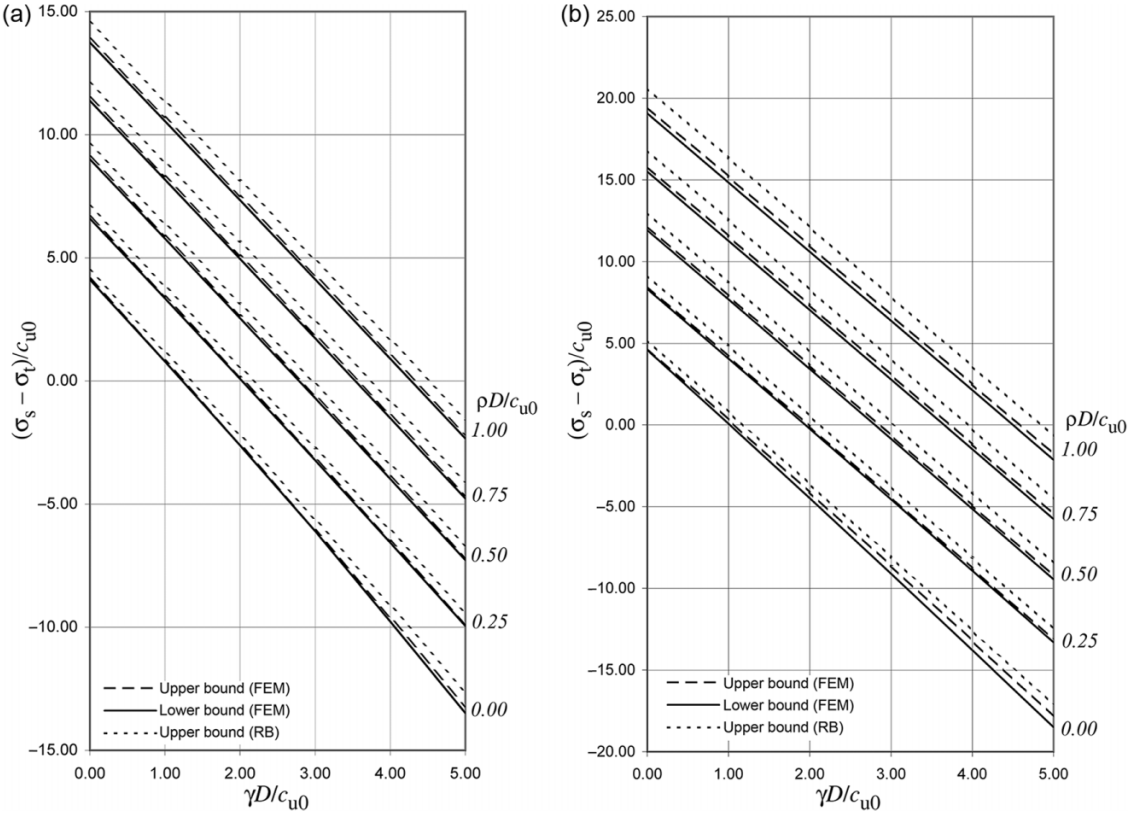

Fig. 6. Results for (*a*) $H/D = 5$; (*b*) $H/D = 6$.

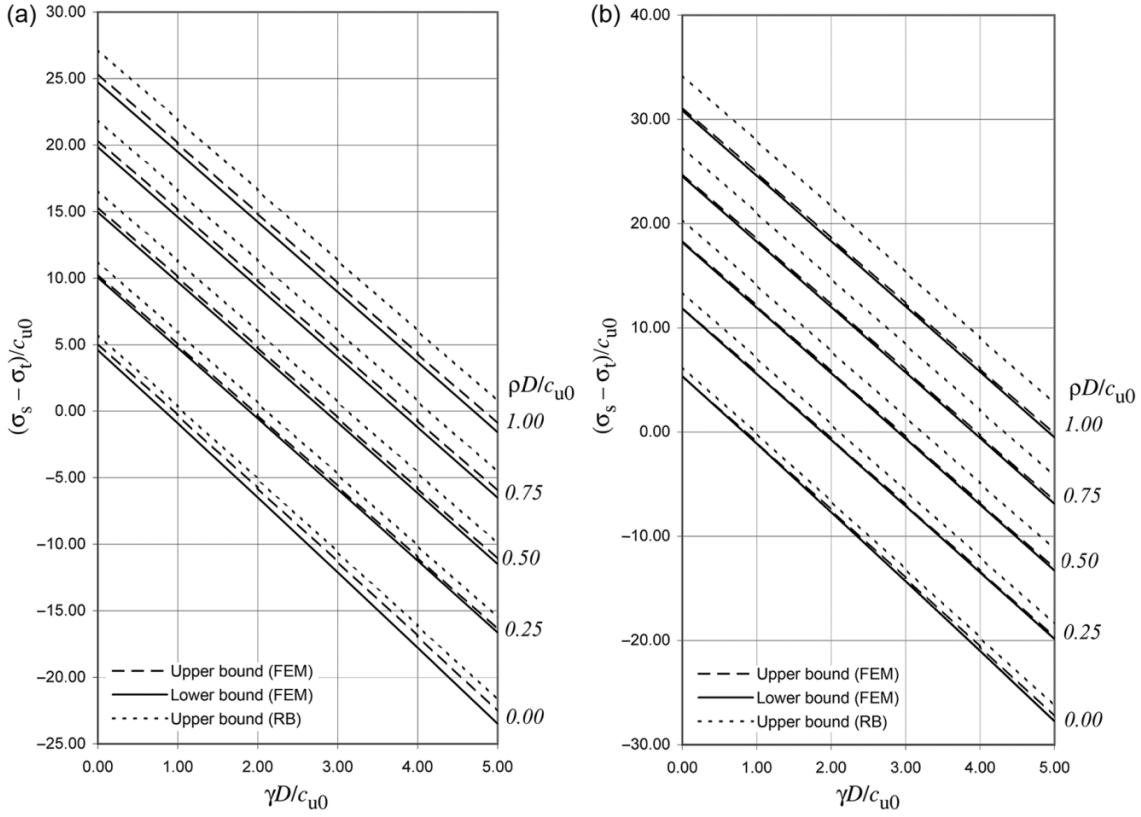

Fig. 7. Results for (*a*) $H/D = 7$; (*b*) $H/D = 8$.

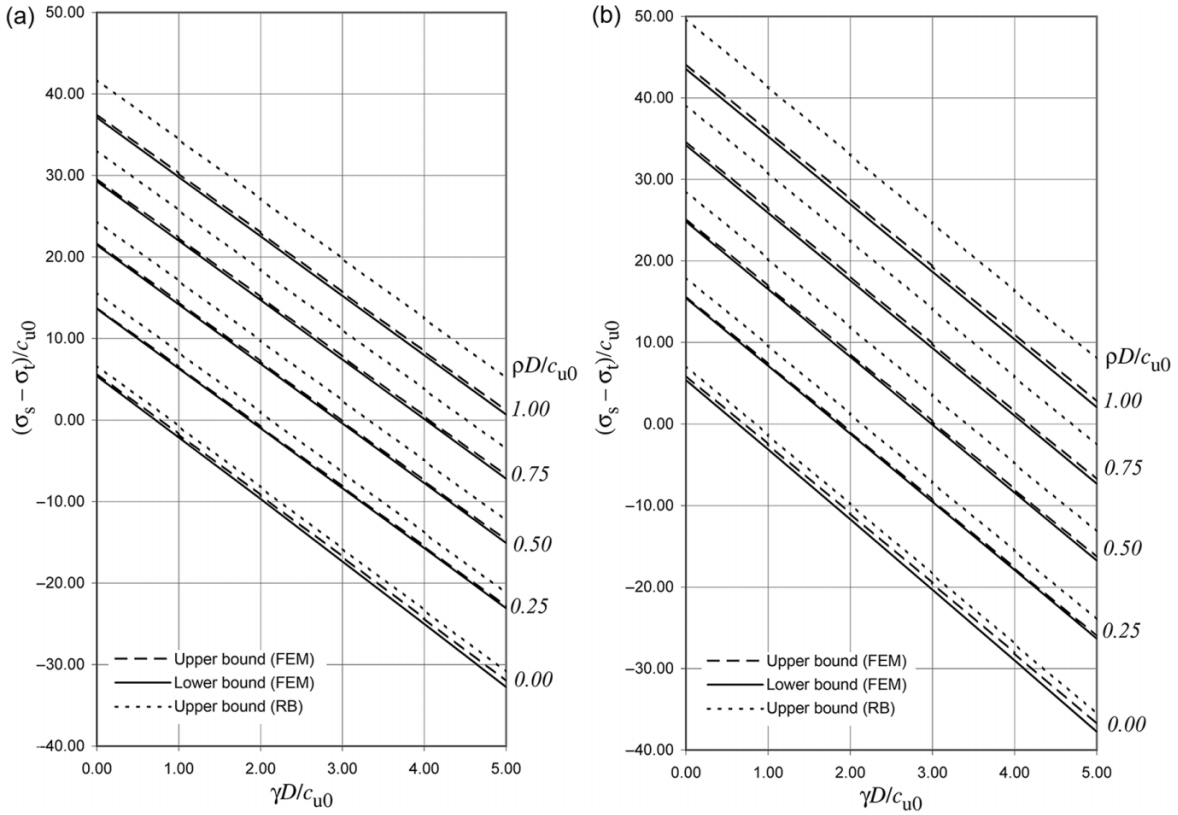

Fig. 8. Results for (*a*) $H/D = 9$; (*b*) $H/D = 10$.

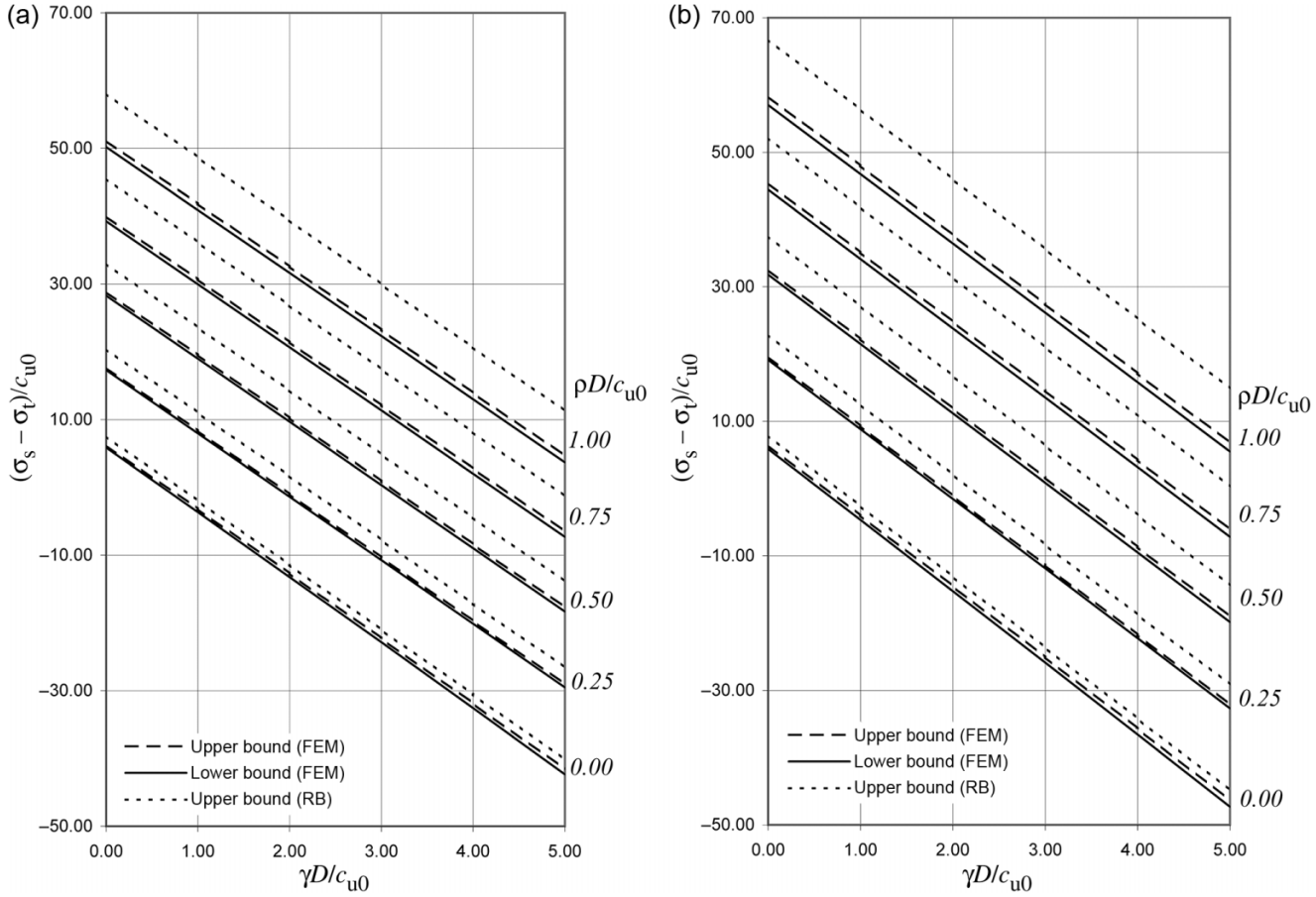

Fig. 9. (*a*) Power dissipation intensity and (*b*) velocity plot for $H/D = 1$, $\gamma D/c_{u0} = 0$, and $\rho D/c_{u0} = 0$.

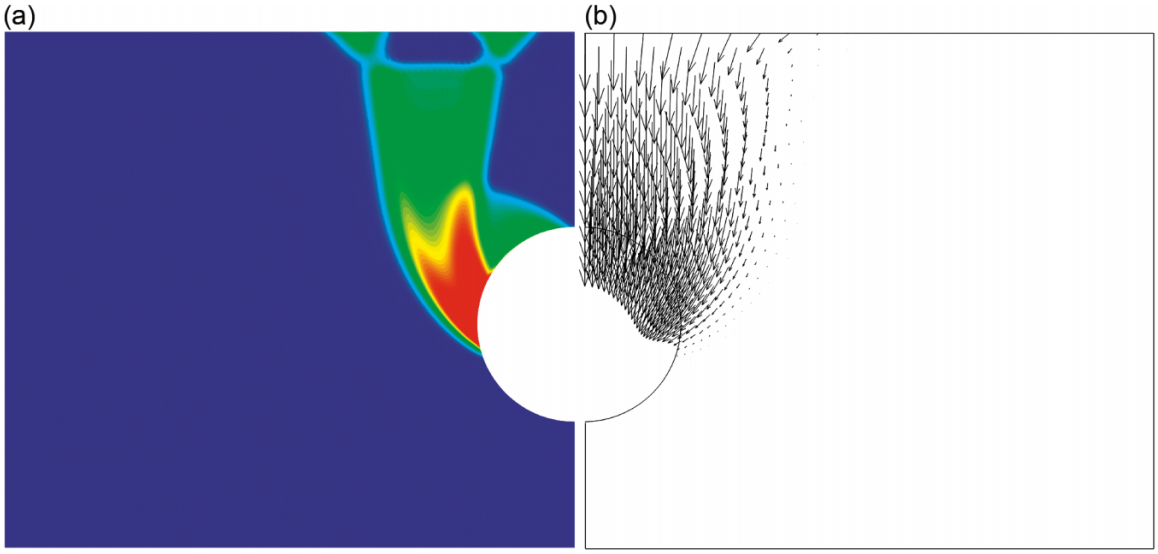

closely match the finite element lower bound solutions. In most instances, the fitted predictions lie below the lower bounds and hence provide conservative estimates. Where this is not the case, the approximation has been tuned to lie below the upper bounds predicted from finite element limit analysis. Although not shown, the accuracy of the predictions is similar for other values of $\gamma D/c_{u0}$, and the equations are thus a useful design tool for practising engineers.

Conclusions

The stability of a circular tunnel in an undrained clay whose shear strength increases linearly with depth has been investigated under plain strain conditions. Stability solutions for a wide range of geometries and soil conditions have been found using both semianalytical upper bound limit analysis and finite element limit analysis. Using these solutions, a

Fig. 10. (*a*) Power dissipation intensity and (*b*) velocity plot for $H/D = 1$, $\gamma D/c_{u0} = 0$, and $\rho D/c_{u0} = 1$.

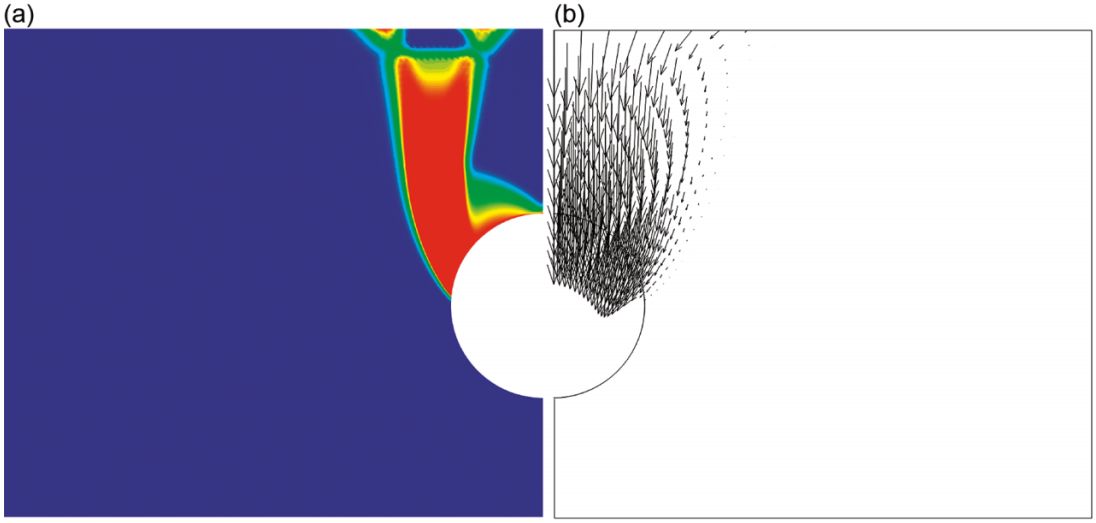

Fig. 11. (*a*) Power dissipation intensity and (*b*) velocity plot for $H/D = 4$, $\gamma D/c_{u0} = 3$, and $\rho D/c_{u0} = 0$.

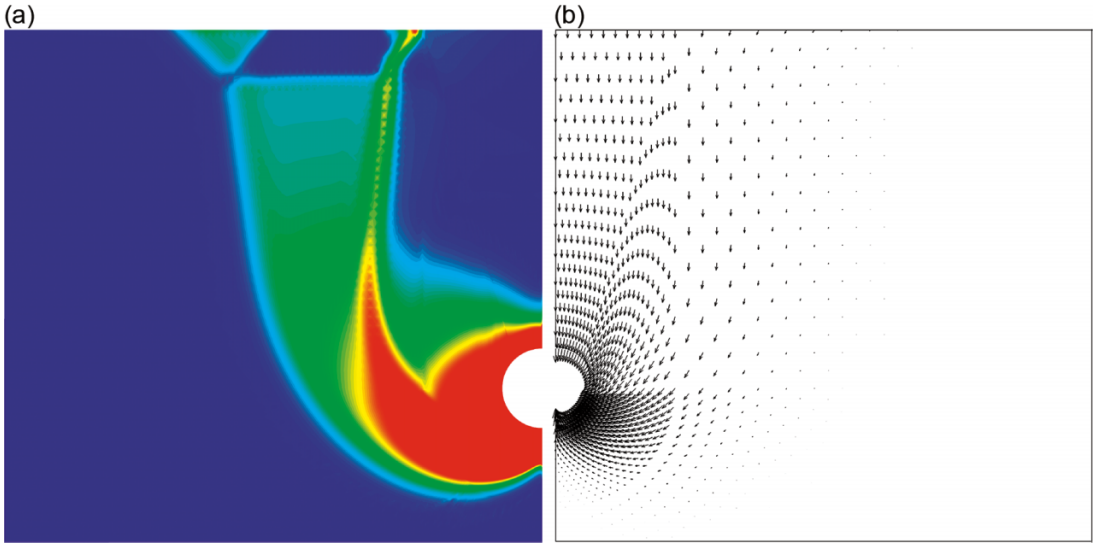

Fig. 12. (*a*) Power dissipation intensity and (*b*) velocity plot for $H/D = 4$, $\gamma D/c_{u0} = 3$, and $\rho D/c_{u0} = 1$.

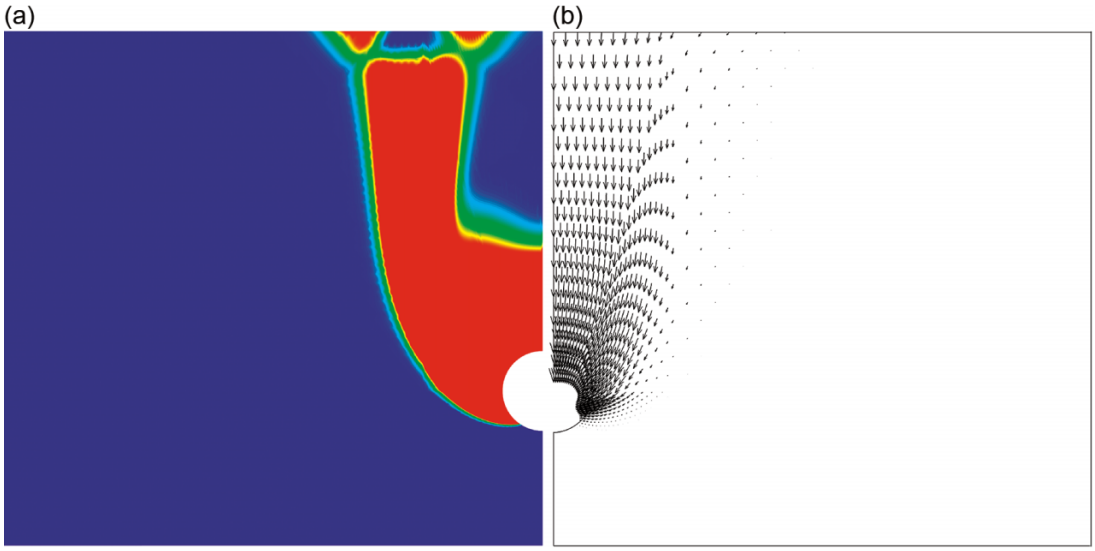

Fig. 13. (*a*) Power dissipation intensity and (*b*) velocity plot for $H/D = 7$, $\gamma D/c_{u0} = 4$, and $\rho D/c_{u0} = 0$.

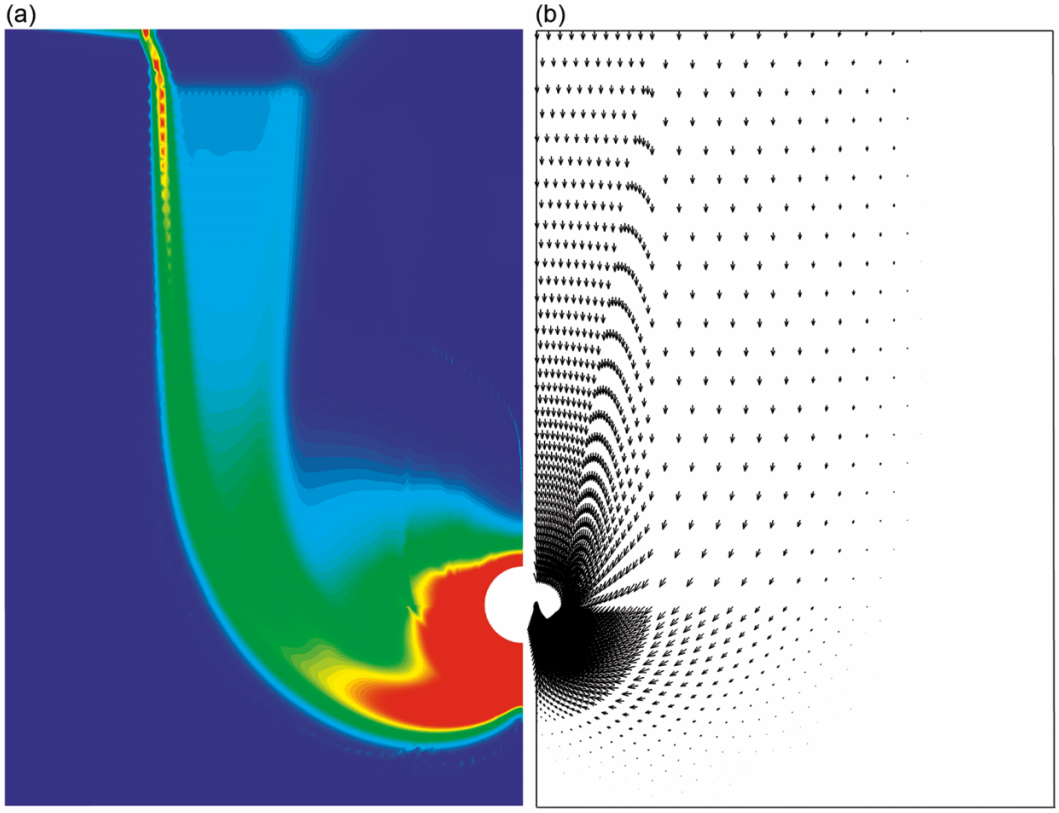

Fig. 14. (*a*) Power dissipation intensity and (*b*) velocity plot for $H/D = 7$, $\gamma D/c_{u0} = 4$, and $\rho D/c_{u0} = 1$.

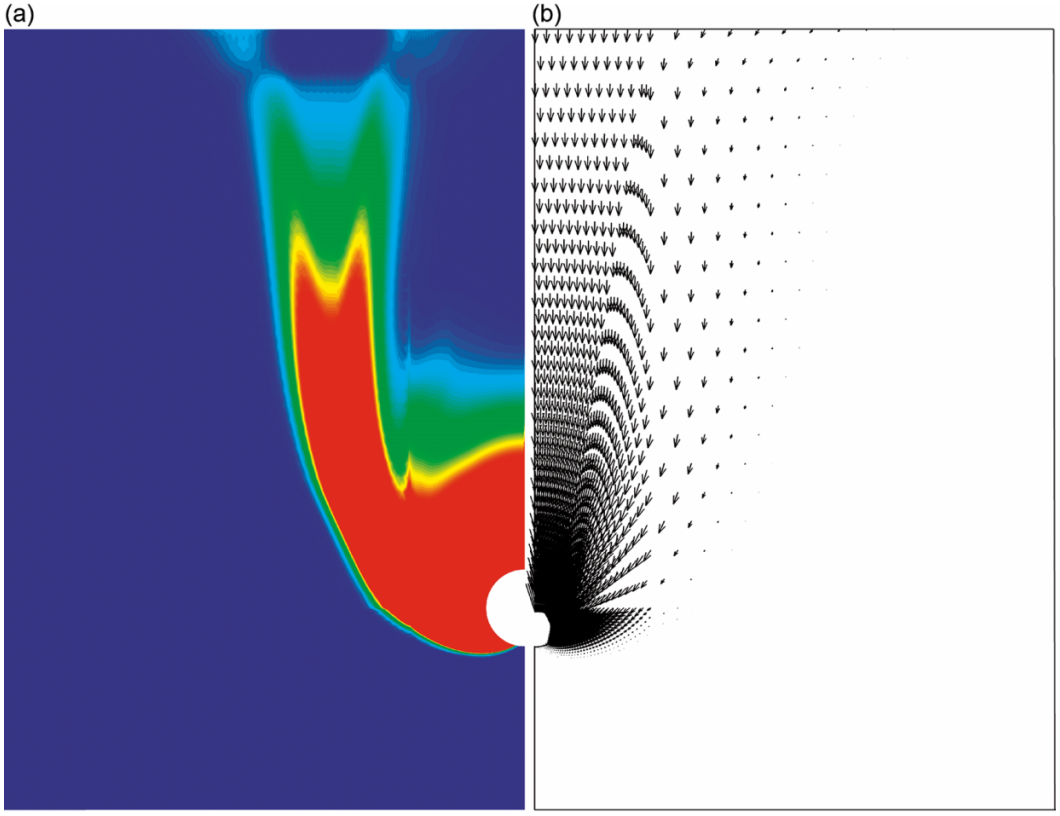

Fig. 15. (*a*) Power dissipation intensity and (*b*) velocity plot for $H/D = 10$, $\gamma D/c_{u0} = 5$, and $\rho D/c_{u0} = 0$.

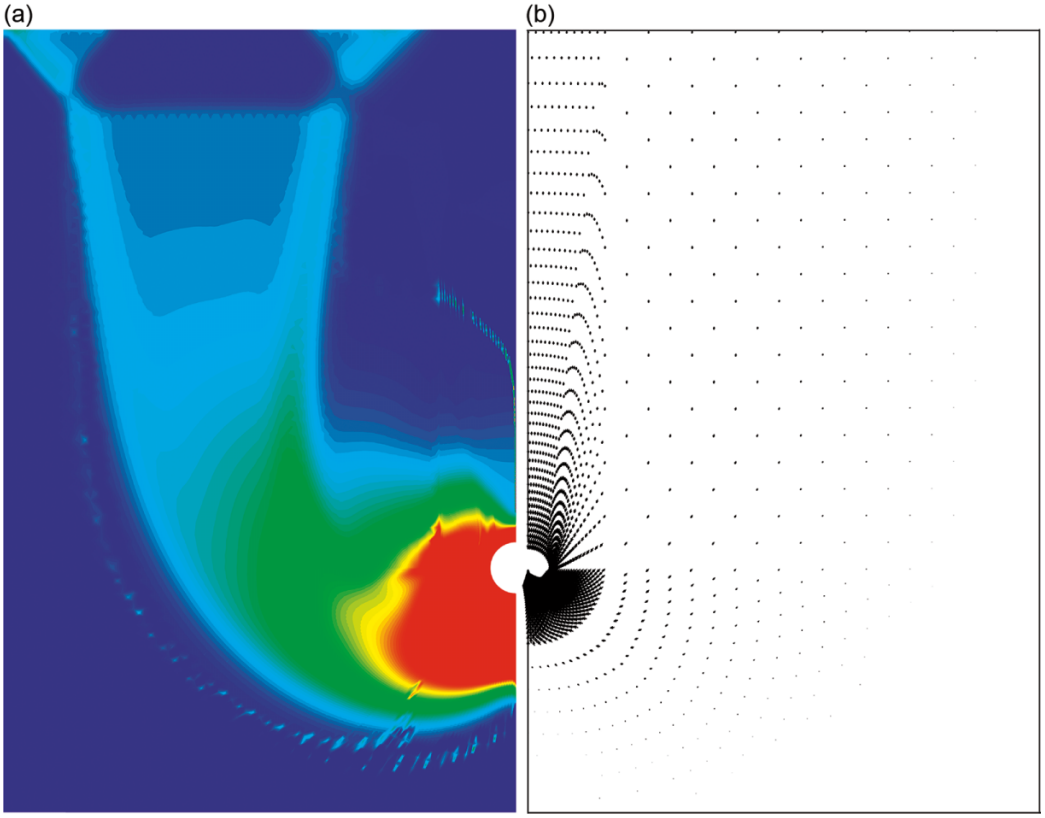

Fig. 16. (*a*) Power dissipation intensity and (*b*) velocity plot for $H/D = 10$, $\gamma D/c_{u0} = 5$, and $\rho D/c_{u0} = 1$.

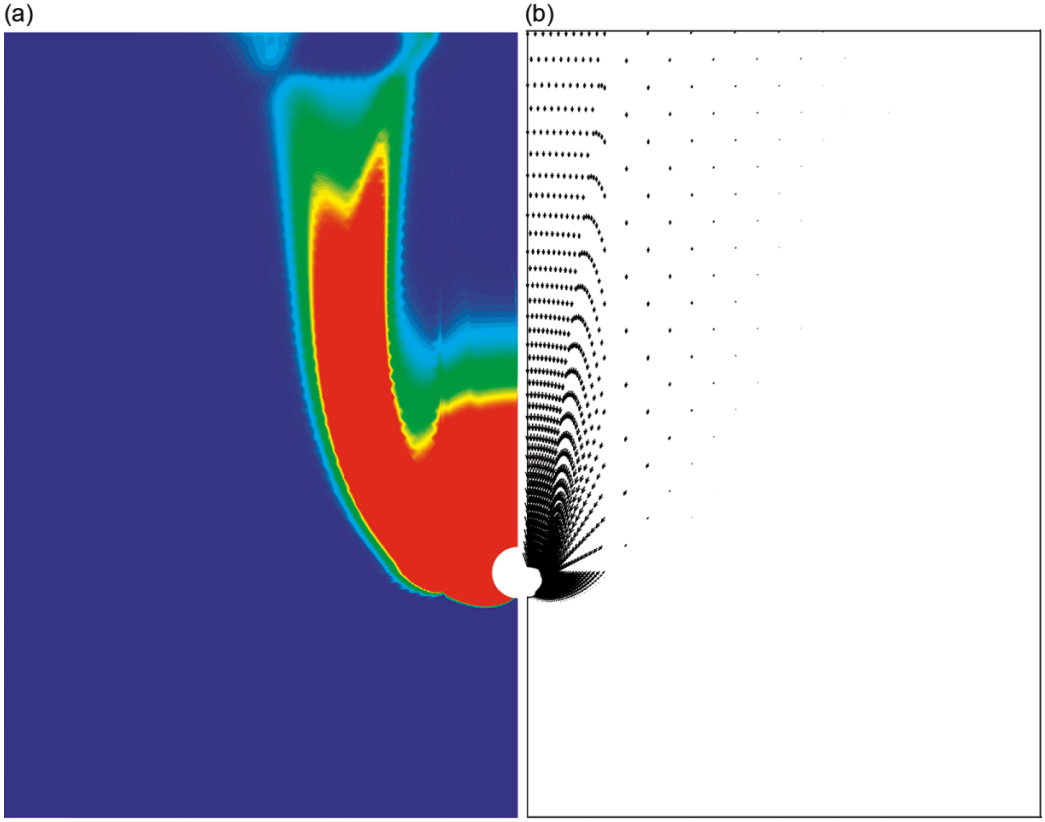

Fig. 17. Comparison of results with published data for $\rho = 0$ and $\gamma D/c_{u0} = 2.6$. LB, lower bound; UB, upper bound.

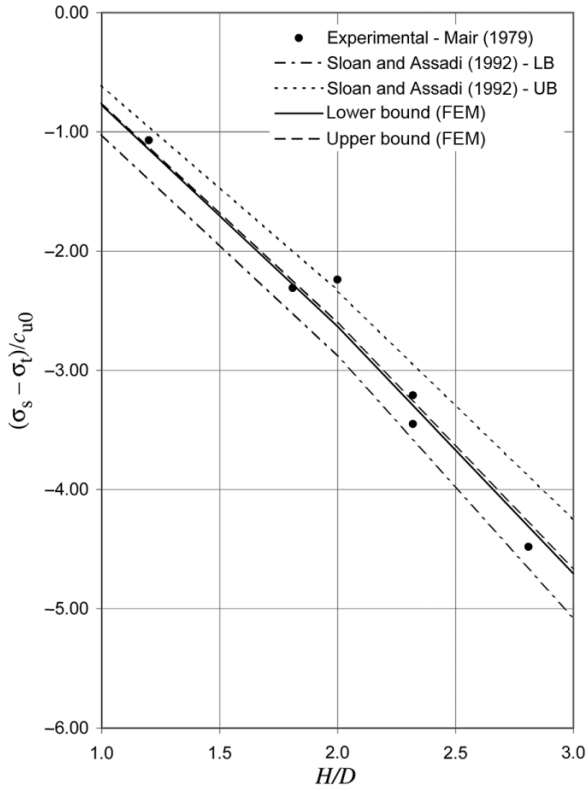

Fig. 18. Comparison of results with those of Sloan and Assadi (1992) for $H/D = 4$.

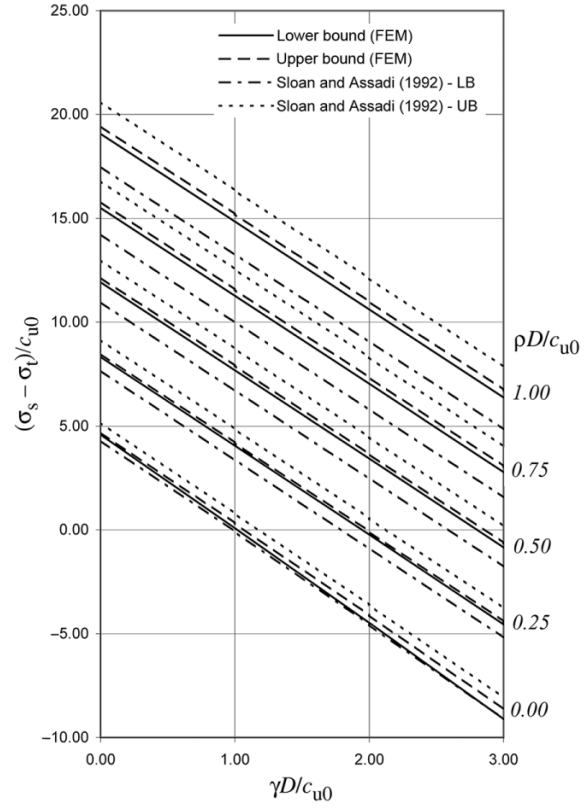

Fig. 19. Stability factor N_0.

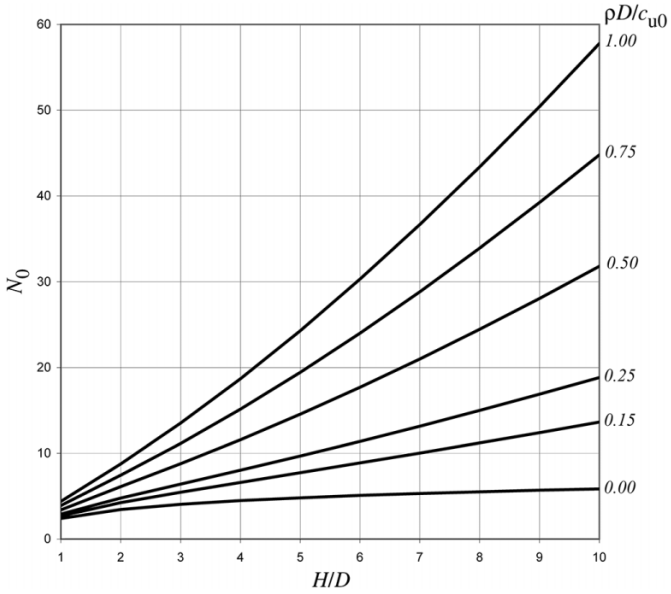

Fig. 20. Comparison of limit analysis and design formula using eqs. [4]–[7] for $\gamma D/c_{u0} = 2$.

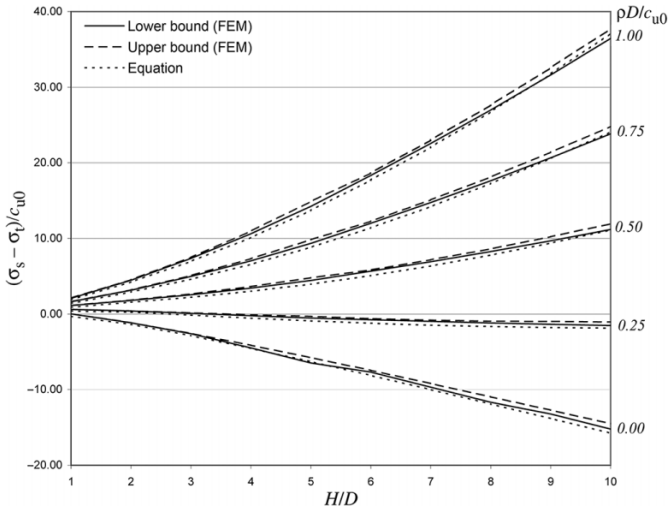

compact set of stability charts that are useful for design purposes has been generated. In addition, an accurate approximate equation for computing tunnel stability has been found by curve-fitting the finite element limit analysis solutions. For the vast majority of cases, this equation will give a slightly conservative prediction of tunnel stability.

The new bounds provide a marked improvement over the results of Sloan and Assadi (1992) when the shear strength of the soil is nonuniform, and also cover a much broader range of soil parameters and tunnel geometries. For the shallow tunnels with $\rho D/c_{u0} \leq 0.25$, the rigid-block methods furnish relatively accurate upper bound solutions for a small amount of computational effort. However, for deep tunnels with high rates of strength increase, these methods are less accurate due to increased complexity of the true collapse mechanism.

Acknowledgements

In conducting the research reported in this paper, the first author was funded by Australian Research Council Discovery (Project DP0771727), while the second author was funded by an Australian Research Council Federation Fellowship (Grant No. FF0455859). The authors are grateful for this support.

References

Atkinson, J.H., and Cairncross, A.M. 1973. Collapse of a shallow tunnel in a Mohr–Coulomb material. *In* Proceedings of the Symposium on the Role of Plasticity in Soil Mechanics, Cambridge, UK, 13–15 September 1973. *Edited by* A.C. Palmer. Cambridge University Engineering Department, University of Cambridge, Cambridge, UK. pp. 202–206.

Atkinson, J.H., and Potts, D.M. 1977. Stability of a shallow circular tunnel in cohesionless soil. Géotechnique, **27**(2): 203–215. doi:10.1680/geot.1977.27.2.203.

Augarde, C.E., Lyamin, A.V., and Sloan, S.W. 2003. Stability of an undrained plane strain heading revisited. Computers and Geotechnics, **30**(5): 419–430. doi:10.1016/S0266-352X(03)00009-0.

Cairncross, A.M. 1973. Deformation around model tunnels in stiff clay. Ph.D. thesis, University of Cambridge, Cambridge, UK.

Chambon, P., and Corté, J.-F. 1994. Shallow tunnels in cohesionless soil: stability of tunnel face. Journal of Geotechnical and Geoenvironmental Engineering, **120**(7): 1148–1165. 10.1061/(ASCE)0733-9410(1994)120:7(1148).

Chen, W.-F. 1975. Limit analysis and soil plasticity. Elsevier Scientific Publishing Company, Amsterdam, the Netherlands.

Davis, E.H., Gunn, M.J., Mair, R.J., and Seneviratine, H.N. 1980. The stability of shallow tunnels and underground openings in cohesive material. Géotechnique, **30**(4): 397–416. doi:10.1680/geot.1980.30.4.397.

Hooke, R., and Jeeves, T.A. 1961. Direct search solution of numerical and statistical problems. Journal of the Association for Computing Machinery, **8**(2): 212–229.

Krabbenhoft, K., Lyamin, A.V., Hjiaj, M., and Sloan, S.W. 2005. A new discontinuous upper bound limit analysis formulation. International Journal for Numerical Methods in Engineering, **63**(7): 1069–1088. doi:10.1002/nme.1314.

Krabbenhoft, K., Lyamin, A.V., and Sloan, S.W. 2007. Formulation and solution of some plasticity problems as conic programs. International Journal of Solids and Structures, **44**(5): 1533–1549. doi:10.1016/j.ijsolstr.2006.06.036.

Leca, E., and Dormieux, L. 1990. Upper and lower bound solutions for the face stability of shallow circular tunnels in frictional material. Géotechnique, **40**(4): 581–606. doi:10.1680/geot.1990.40.4.581.

Lyamin, A.V., and Sloan, S.W. 2000. Stability of a plane strain circular tunnel in a cohesive–frictional soil. *In* Proceedings of the J.R. Booker Memorial Symposium, Sydney, Australia, 16–17 November 2000. Balkema, Rotterdam, the Netherlands. *Edited by* D.W. Smith and J.P. Carter. pp. 139–153.

Lyamin, A.V., and Sloan, S.W. 2002*a*. Lower bound limit analysis using nonlinear programming. International Journal for Numerical Methods in Engineering, **55**(5): 573–611. doi:10.1002/nme.511.

Lyamin, A.V., and Sloan, S.W. 2002*b*. Upper bound limit analysis using linear finite elements and nonlinear programming. International Journal for Numerical and Analytical Methods in Geomechanics, **26**(2): 181–216. doi:10.1002/nag.198.

Mair, R.J. 1979. Centrifugal modelling of tunnel construction in soft clay. Ph.D. thesis, University of Cambridge, Cambridge, UK.

Muhlhaus, H.B. 1985. Lower bound solutions for circular tunnels in two and three dimensions. Rock Mechanics and Rock Engineering, **18**(1): 37–52. doi:10.1007/BF01020414.

Seneviratne, H.N. 1979. Deformations and pore-pressures around model tunnels in soft clay. Ph.D. thesis, University of Cambridge, Cambridge, UK.

Sloan, S.W. 1988. Lower bound limit analysis using finite elements and linear programming. International Journal for Numerical and Analytical Methods in Geomechanics, **12**(1): 61–77. doi:10.1002/nag.1610120105.

Sloan, S.W. 1989. Upper bound limit analysis using finite elements and linear programming. International Journal for Numerical and Analytical Methods in Geomechanics, **13**(3): 263–282. doi:10.1002/nag.1610130304.

Sloan, S.W., and Assadi, A. 1992. The stability of tunnels in soft ground. *In* Proceedings of the Wroth Memorial Symposium on Predictive Soil Mechanics, Oxford, UK, 27–29 July 1992. *Edited by* G.T. Houlsby. Thomas Telford Ltd., London. pp. 644–663.

Appendix A

Tables A1 and A2 in this appendix give the values used to generate the stability charts in Figs. 4–8. Table A3 contains the values for N_0 that were used to generate the chart in Fig. 18.

Table A1. Stability bounds for a circular tunnel with $\gamma D/c_{u0} = 0$–2.

		$\gamma D/c_{u0} = 0$			$\gamma D/c_{u0} = 1$			$\gamma D/c_{u0} = 2$		
H/D	$\rho D/c_{u0}$	FE lower bound	FE upper bound	RB upper bound	FE lower bound	FE upper bound	RB upper bound	FE lower bound	FE upper bound	RB upper bound
1.0	0.00	2.43	2.45	2.53	1.25	1.26	1.36	0.01	0.03	0.15
	0.25	2.93	2.95	3.03	1.78	1.80	1.89	0.61	0.63	0.72
	0.50	3.40	3.43	3.51	2.27	2.30	2.38	1.13	1.15	1.24
	0.75	3.87	3.90	3.98	2.75	2.78	2.86	1.62	1.65	1.73
	1.00	4.33	4.37	4.44	3.22	3.25	3.33	2.10	2.13	2.21
2.0	0.00	3.45	3.48	3.68	1.17	1.20	1.41	–1.17	–1.15	–0.91
	0.25	4.83	4.88	5.10	2.63	2.67	2.89	0.39	0.43	0.65
	0.50	6.17	6.23	6.47	3.99	4.04	4.28	1.78	1.84	2.08
	0.75	7.49	7.56	7.82	5.32	5.38	5.64	3.14	3.20	3.46
	1.00	8.80	8.87	9.16	6.64	6.71	6.99	4.46	4.54	4.81
3.0	0.00	4.12	4.16	4.50	0.79	0.84	1.18	–2.62	–2.57	–2.20
	0.25	6.60	6.68	7.11	3.36	3.44	3.85	0.09	0.17	0.58
	0.50	9.00	9.11	9.62	5.79	5.90	6.39	2.55	2.66	3.15
	0.75	11.38	11.52	12.10	8.18	8.31	8.88	4.96	5.10	5.66
	1.00	13.75	13.91	14.57	10.55	10.71	11.36	7.34	7.51	8.14
4.0	0.00	4.59	4.69	5.17	0.09	0.33	0.81	–4.48	–4.11	–3.61
	0.25	8.32	8.48	9.15	4.06	4.21	4.86	–0.23	–0.09	0.56
	0.50	11.93	12.16	12.99	7.69	7.91	8.73	3.44	3.66	4.46
	0.75	15.51	15.80	16.80	11.28	11.57	12.56	7.04	7.33	8.30
	1.00	19.07	19.44	20.60	14.85	15.22	16.36	10.62	10.98	12.11
5.0	0.00	4.59	5.09	5.75	–0.91	–0.30	0.35	–6.47	–5.77	–5.09
	0.25	10.04	10.29	11.25	4.76	5.01	5.94	–0.54	–0.29	0.61
	0.50	14.96	15.35	16.59	9.70	10.09	11.30	4.43	4.81	6.01
	0.75	19.84	20.37	21.89	14.60	15.12	16.62	9.34	9.86	11.33
	1.00	24.71	25.38	27.17	19.47	20.14	21.90	14.23	14.88	16.63
6.0	0.00	5.36	5.42	6.25	–1.10	–0.98	–0.15	–7.68	–7.45	–6.63
	0.25	11.86	11.98	13.42	5.57	5.69	7.10	–0.75	–0.62	0.75
	0.50	18.22	18.40	20.39	11.94	12.13	14.09	5.66	5.84	7.77
	0.75	24.54	24.79	27.33	18.28	18.52	21.03	12.01	12.25	14.73
	1.00	30.86	31.16	34.24	24.60	24.91	27.95	18.33	18.64	21.65
7.0	0.00	5.40	5.71	6.71	–2.11	–1.70	–0.73	–9.68	–9.18	–8.21
	0.25	13.65	13.82	15.67	6.34	6.52	8.32	–0.98	–0.80	0.96
	0.50	21.49	21.74	24.40	14.21	14.47	17.07	6.91	7.18	9.74
	0.75	29.30	29.64	33.09	22.03	22.37	25.77	14.74	15.09	18.45
	1.00	37.10	37.53	41.76	29.83	30.27	34.45	22.55	22.99	27.13
8.0	0.00	5.40	5.97	7.14	–3.11	–2.45	–1.33	–11.68	–10.94	–9.83
	0.25	15.46	15.69	17.99	7.15	7.38	9.63	–1.18	–0.94	1.26
	0.50	24.86	25.21	28.60	16.56	16.93	20.25	8.26	8.63	11.90
	0.75	34.21	34.71	39.17	25.93	26.43	30.82	17.64	18.14	22.48
	1.00	43.56	44.19	49.70	35.28	35.91	41.37	26.99	27.63	33.05
9.0	0.00	5.87	6.23	7.52	–3.64	–3.20	–1.95	–13.22	–12.70	–11.43
	0.25	17.30	17.64	20.39	7.98	8.34	11.01	–1.36	–0.98	1.62
	0.50	28.30	28.82	32.98	19.00	19.53	23.62	9.68	10.24	14.25
	0.75	39.26	39.98	45.53	29.97	30.70	36.17	20.67	21.41	26.81
	1.00	50.22	51.13	58.05	40.93	41.85	48.70	31.63	32.56	39.34
10.0	0.00	5.86	6.44	7.88	–4.65	–4.00	–2.60	–15.22	–14.50	–13.09
	0.25	19.15	19.60	22.85	8.83	9.29	12.46	–1.51	–1.03	2.06
	0.50	31.82	32.53	37.51	21.51	22.23	27.14	11.18	11.93	16.76
	0.75	44.44	45.42	52.12	34.14	35.13	41.77	23.83	24.83	31.40
	1.00	57.03	58.29	66.74	46.76	48.01	56.38	36.45	37.72	46.01

Table A2. Stability bounds for a circular tunnel with $\gamma D/c_{u0} = 3$–5.

		$\gamma D/c_{u0} = 3$			$\gamma D/c_{u0} = 4$			$\gamma D/c_{u0} = 5$		
H/D	$\rho D/c_{u0}$	FE lower bound	FE upper bound	RB upper bound	FE lower bound	FE upper bound	RB upper bound	FE lower bound	FE upper bound	RB upper bound
1.0	0.00	–1.30	–1.29	–1.12	–2.72	–2.70	–2.47	–4.22	–4.20	–3.89
	0.25	–0.60	–0.58	–0.47	–1.86	–1.83	–1.70	–3.17	–3.15	–2.97
	0.50	–0.04	–0.02	0.08	–1.23	–1.21	–1.10	–2.46	–2.44	–2.31
	0.75	0.47	0.50	0.59	–0.69	–0.66	–0.56	–1.87	–1.85	–1.74
	1.00	0.96	1.00	1.08	–0.18	–0.15	–0.06	–1.34	–1.31	–1.21
2.0	0.00	–3.60	–3.58	–3.28	–6.11	–6.08	–5.71	–8.68	–8.65	–8.20
	0.25	–1.88	–1.85	–1.61	–4.20	–4.16	–3.90	–6.57	–6.53	–6.23
	0.50	–0.44	–0.39	–0.14	–2.68	–2.63	–2.38	–4.96	–4.91	–4.64
	0.75	0.94	1.00	1.26	–1.28	–1.22	–0.95	–3.51	–3.45	–3.18
	1.00	2.28	2.35	2.63	0.08	0.15	0.43	–2.13	–2.06	–1.77
3.0	0.00	–6.10	–6.05	–5.63	–9.77	–9.60	–9.11	–13.48	–13.21	–12.63
	0.25	–3.22	–3.14	–2.72	–6.56	–6.49	–6.05	–9.95	–9.87	–9.40
	0.50	–0.70	–0.59	–0.11	–3.97	–3.87	–3.38	–7.27	–7.16	–6.67
	0.75	1.73	1.87	2.42	–1.51	–1.38	–0.83	–4.77	–4.63	–4.08
	1.00	4.13	4.29	4.92	0.90	1.06	1.69	–2.34	–2.17	–1.55
4.0	0.00	–9.10	–8.63	–8.08	–13.77	–13.21	–12.58	–18.49	–17.84	–17.13
	0.25	–4.55	–4.41	–3.77	–8.91	–8.76	–8.12	–13.30	–13.15	–12.49
	0.50	–0.84	–0.62	0.18	–5.13	–4.91	–4.12	–9.44	–9.23	–8.44
	0.75	2.79	3.08	4.03	–1.47	–1.19	–0.24	–5.75	–5.46	–4.53
	1.00	6.38	6.74	7.85	2.13	2.49	3.59	–2.12	–1.77	–0.68
5.0	0.00	–12.10	–11.30	–10.59	–17.77	–16.90	–16.12	–23.48	–22.55	–21.68
	0.25	–5.87	–5.63	–4.74	–11.23	–10.99	–10.10	–16.62	–16.38	–15.49
	0.50	–0.85	–0.48	0.70	–6.16	–5.78	–4.62	–11.48	–11.11	–9.95
	0.75	4.07	4.58	6.04	–1.20	–0.70	0.75	–6.49	–5.99	–4.56
	1.00	8.97	9.62	11.35	3.71	4.35	6.07	–1.57	–0.93	0.77
6.0	0.00	–14.31	–13.99	–13.16	–21.00	–20.60	–19.70	–27.73	–27.26	–26.26
	0.25	–7.09	–6.95	–5.62	–13.46	–13.30	–12.00	–19.86	–19.68	–18.40
	0.50	–0.64	–0.45	1.44	–6.96	–6.76	–4.89	–13.29	–13.08	–11.24
	0.75	5.72	5.97	8.41	–0.57	–0.32	2.10	–6.87	–6.61	–4.23
	1.00	12.06	12.37	15.35	5.78	6.09	9.04	–0.51	–0.19	2.73
7.0	0.00	–17.32	–16.74	–15.76	–25.01	–24.35	–23.29	–32.73	–32.01	–30.88
	0.25	–8.33	–8.13	–6.41	–15.70	–15.49	–13.82	–23.10	–22.88	–21.23
	0.50	–0.40	–0.13	2.40	–7.72	–7.44	–4.96	–15.06	–14.77	–12.32
	0.75	7.45	7.81	11.12	0.15	0.51	3.79	–7.17	–6.79	–3.55
	1.00	15.27	15.71	19.81	7.98	8.43	12.48	0.68	1.13	5.15
8.0	0.00	–20.32	–19.50	–18.39	–29.01	–28.12	–26.95	–37.74	–36.79	–35.53
	0.25	–9.54	–9.29	–7.14	–17.92	–17.65	–15.53	–26.32	–26.04	–23.96
	0.50	–0.06	0.32	3.54	–8.39	–8.00	–4.82	–16.73	–16.33	–13.19
	0.75	9.33	9.84	14.13	1.02	1.54	5.79	–7.30	–6.77	–2.57
	1.00	18.70	19.34	24.70	10.40	11.04	16.36	2.07	2.74	8.01
9.0	0.00	–22.86	–22.26	–21.01	–32.58	–31.88	–30.54	–42.32	–41.56	–40.18
	0.25	–10.72	–10.32	–7.77	–20.11	–19.68	–17.17	–29.50	–29.06	–26.57
	0.50	0.36	0.93	4.87	–8.99	–8.38	–4.49	–18.33	–17.70	–13.88
	0.75	11.35	12.11	17.44	2.03	2.81	8.09	–7.29	–6.50	–1.29
	1.00	22.33	23.27	29.98	13.02	13.97	20.62	3.70	4.67	11.26
10.0	0.00	–25.86	–25.07	–23.64	–36.57	–35.69	–34.22	–47.29	–46.37	–44.84
	0.25	–11.88	–11.38	–8.34	–22.26	–21.74	–18.74	–32.67	–32.13	–29.15
	0.50	0.85	1.62	6.38	–9.49	–8.70	–3.90	–19.85	–19.03	–14.40
	0.75	13.51	14.53	21.02	3.18	4.23	10.76	–7.16	–6.09	0.33
	1.00	26.14	27.42	35.64	15.82	17.12	25.26	5.49	6.82	14.89

Table A3. N_0 values calculated using eq. [4] and used to generate the design chart (Fig. 18).

	N_0				
H/D	$\rho D/c_{u0}$ = 0.00	$\rho D/c_{u0}$ = 0.25	$\rho D/c_{u0}$ = 0.50	$\rho D/c_{u0}$ = 0.75	$\rho D/c_{u0}$ = 1.00
1.0	2.40	2.90	3.40	3.90	4.40
2.0	3.44	4.77	6.10	7.44	8.77
3.0	4.05	6.41	8.78	11.14	13.51
4.0	4.48	8.03	11.58	15.13	18.69
5.0	4.81	9.68	14.55	19.42	24.29
6.0	5.09	11.39	17.69	23.99	30.29
7.0	5.32	13.16	20.99	28.83	36.66
8.0	5.52	14.98	24.45	33.91	43.38
9.0	5.70	16.88	28.06	39.24	50.42
10.0	5.85	18.83	31.81	44.79	57.76